Electronic Supplementary Material (ESI) for Journal of Materials Chemistry C.

Co-crystallization strategy toward high-performance N-type organic semiconductor switched from P-type planar azaacene derivative

Zongrui Wang,*[a,b] Renping Li,[c] Kexiang Zhao,[d] Fei Yu,[b] Jianfeng Zhao,*[c] Yonggang Zhen,[a] Qichun Zhang*[e,f]

[a] School of Materials Science and Engineering, Beijing University of Chemical Technology, Chaoyang District North Third Ring Road 15, Beijing 100029, P. R. China. E-mail: wangzr@mail.buct.edu.cn

[b] School of Materials Science and Engineering, Nanyang Technological University, Singapore 639798, Singapore.

[c] Institute of Advanced Materials (IAM), Nanjing Tech University, Nanjing 210000, P. R. China. E-mail: iamjfzhao@njtech.edu.cn

[d] College of Chemistry and Molecular Engineering, Peking University, Beijing 100871, P. R. China

[e] Department of Materials Science and Engineering, City University of Hong Kong, Tat Chee Avenue, Kowloon, Hong Kong SAR 999077, P. R. China. E-mail: qiczhang@cityu.edu.hk.

[f] Center of Super-Diamond and Advanced Films (COSDAF), City University of Hong Kong, Tat Chee Avenue, Kowloon, Hong Kong SAR 999077, P. R. China

Experimental section:

***Materials and Chemicals*:** 8,8,18,18-tetramethyl-8,18-dihydroindolo[1,2,3-*fg*]indolo[3',2',1':8,1]quinolino[2,3-*b*]acridine (TMIQ) was synthesized as detailed in Scheme S1. 2,3,5,6-Tetrafluoro-7,7,8,8-tetracyanoquinodimethane (F_4TCNQ) was purchased from Sigma-Aldrich Co. Dichloromethane (CH_2Cl_2) and ohter commonly-used solvents were commercially purchased from Aik Moh Solvex (M) Sdn Bhd. All of the chemicals were direclty used without further purification.

***Crystals Growth and Characterization*:** Single crystal of TMIQ and cocrystal of TMF4TQ were prepared by solution-processed method. Specifically, TMIQ and F4TCNQ were mixed in a molar ratio of 1:1 and dissolved in CH_2Cl_2 solvent, and then black rod cocrystals were obtained by rapid vaporization solvent under ambient conditions. Likewise, black rod crystals of TMIQ were also prepared from CH_2Cl_2 solution by rapid vaporization mehod. Single-crystal structure data of TMIQ were collected from a Bruker D8 VENTURE X-ray diffractometer with a large area CCD detector by using graphite monochromated Mo-Kα radiation (λ = 0.71073 Å). The structure was solved and refined by SHELXT 2014/5 program on OLEX2.[1-3] Single-crystal structure data of TMF4TQ were collected from a BRUKER-APEX III X-ray diffractometer with a large area CCD detector by using graphite monochromated Mo-Kα radiation (λ = 0.71073 Å). The structure was solved and refined by SHELXL-2018/3 program.[4-6]

UV-Vis spectra and The UV-Vis absorption and fluorescence spectra were recorded on a Shimadzu UV-1750 and Hitachi F-4600 spectrophotometer, respectively. UV-Vis-

NIR absorption spectra were conducted on a UV-Vis-NIR Lambda 950. Cyclic voltammetry (CV) curves were measured on CHI 760E. Fourier transform infrared spectroscopy (FTIR) was taken on Spectrum GX FTIR Spectrometer. PXRD patterns of powder and micro/nanocrystal were recorded on D8/max 2500 with Cu Kα source (κ = 1.541 Å). Field emission scanning electron microscopy (FESEM) images were obtained by a JEOL/JSM-7600F at an accelerating voltage of 5 kV. Energy dispersive X-ray spectroscopy (EDS) elemental mapping was collected by the same instrument at an accelerating voltage of 15 kV. X-ray photoelectron spectroscopy (XPS, KRATOS Axis Ultra DLD spectrometer) was conducted with a monochromatized Al Kα X-ray source (1486.6 eV) and an analyzer pass energy of 20 eV at take-off angles of 90º.

Device Fabrication and Characterization: SiO_2/Si substrates (300 nm thick SiO_2, C_i = 11 nF/cm^2) were successively cleaned with deionized water, piranha solution (H_2SO_4:H_2O_2 = 7:3), deionized water and isopropanol. Thereafter, n-octadecyltrichlorosilane (OTS) was used to modify the SiO_2/Si substrates by vapor-deposition method to reduce the electron traps. Micro/nano-cocrystals were directly self-assembled on the OTS-modified substrates by the drop-casting method from their respective CH_2Cl_2 solution. Top S/D contacts of gold electrodes were deposited by evaporating gold through the“organic ribbon masks”. [7]

I-V characteristics of the fabricated organic single-crystal field-effect transistors (SCFETs) were obtained from a Keithley 4200 SCS semiconductor parameter analyzer and a Micromanipulator probe station in a clean and shielded box at ambient atmosphere. The mobility is calculated from the saturation region with the following equation: $I_{DS} = (W/2L)C_i\mu_{FET}(V_G - V_T)^2$, from the linear region with the following equation: $I_{DS} = (W/L)C_i\mu_{FET}(V_G - V_T)V_{SD}$, where I_{DS}, W, L, μ_{FET}, and C_i are the drain-source current, channel width, channel length, field-effect mobility and capacitance per unit area of the gate dielectric layer, respectively, and V_G and V_T are the gate and threshold voltage, respectively.

DFT Calculations**:** All theoretical calculations were carried out at the Density Functional Theory (DFT) level of theory using the hybrid B3LYP/6-31G** exchange-correlation functional [8-10] implemented on the Gaussian 09 program. [11] A quadratic convergence method was employed in the SCF process.[12] The triple-ζ quality basis set proposed by Ahlrichs and coworkers has been used for all atoms.[13] Calculations were performed on the complexes built from the experimentally determined geometries with H atoms optimization.

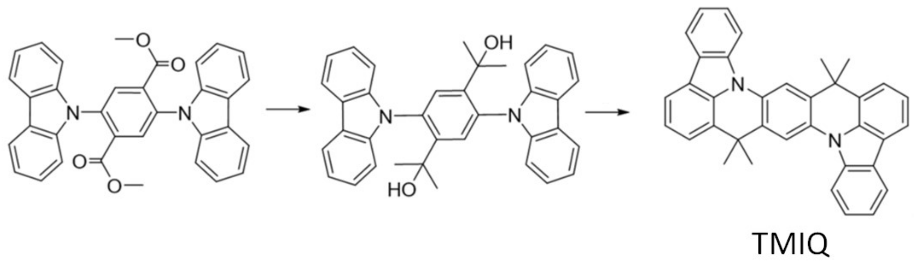

Scheme S1. The synthesis procedure of TMIQ.[14]

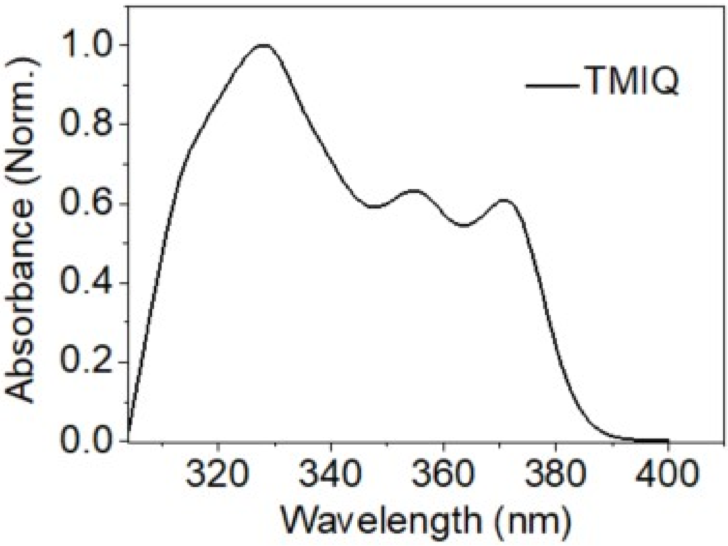

Figure S1. The UV-Vis absorbance spectra of TMIQ in CH_2Cl_2 (10^{-5} mol/L).

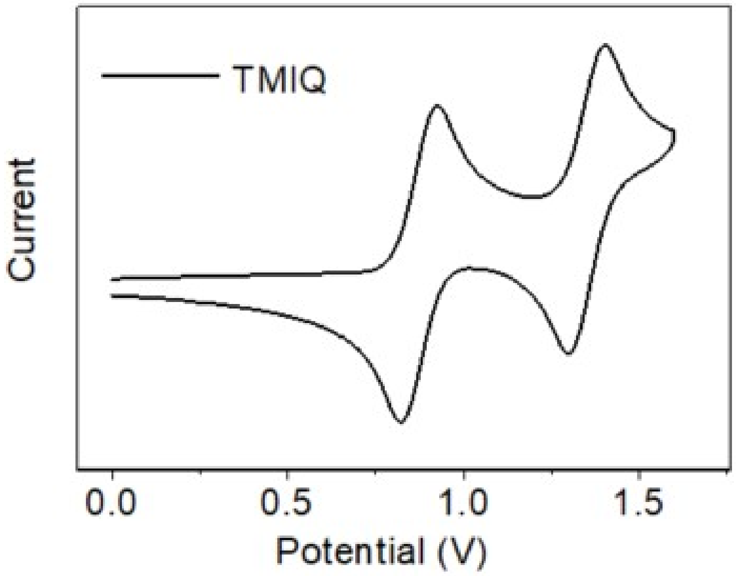

Figure S2. The cyclic voltammetry (CV) curve of TMIQ in CH_2Cl_2 solution (10^{-5} mol/L) containing 0.1 mol/L Bu_4NPF_6 electrolyte.

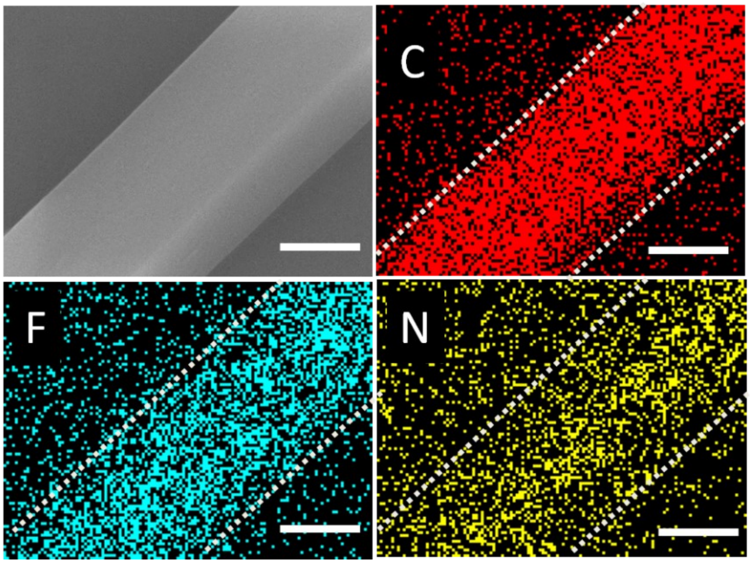

Figure S3. SEM images and X-ray mapping of element carbon (C), fluorine (F) and nitrogen (N) for cocrystal of TMF4TQ.

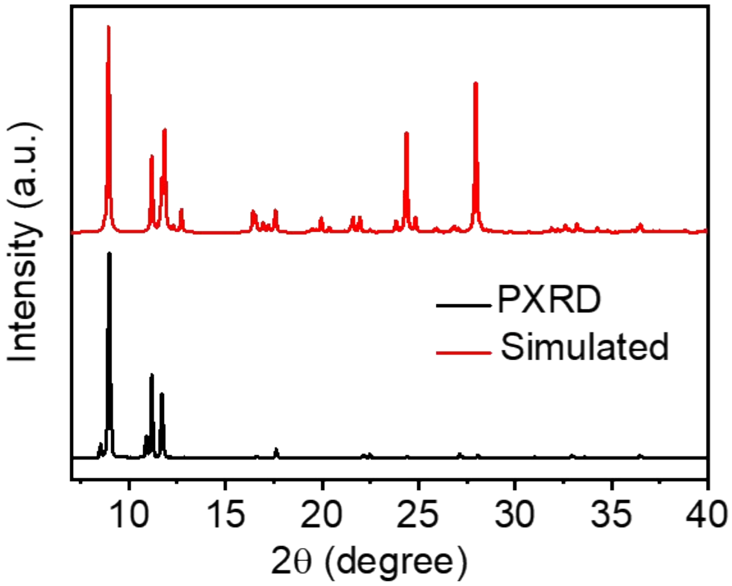

Figure S4. XRD profiles of powders for cocrystal TMF4TQ and its corresponding simulated PXRD curves from SCXRD.

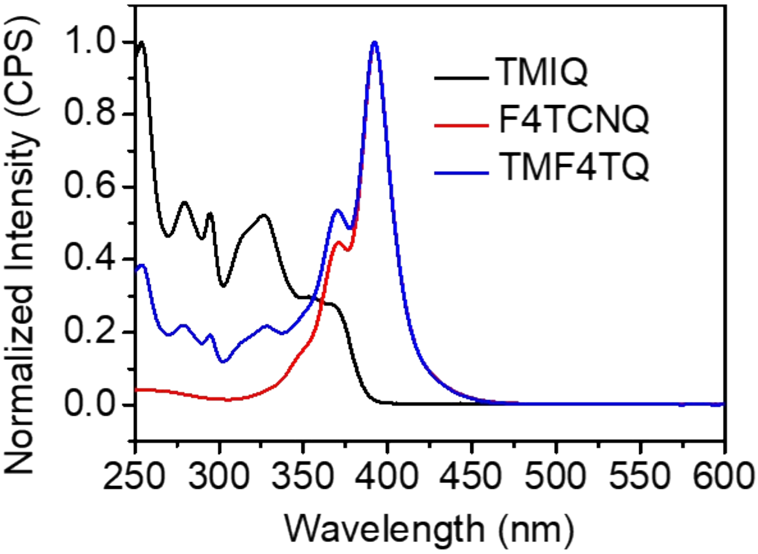

Figure S5. UV-Vis absorbance spectra of TMIQ, F_4TCNQ and TMIQ-F4TCNQ mixture with the molar ratio of 1:1 in CH_2Cl_2.

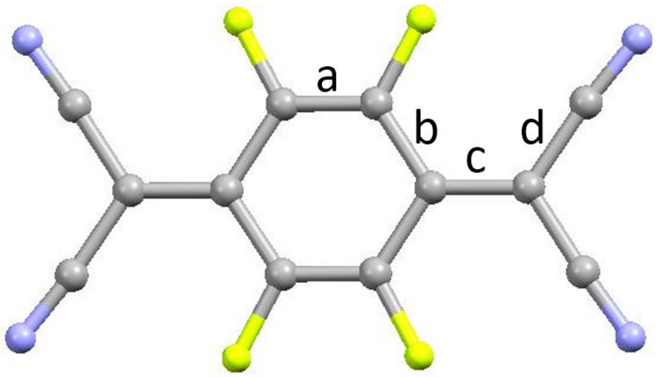

Figure S6. The bond lengths of F_4TCNQ in TMF4TQ complex.

Degree of charge transfer:

Due that the bond lengths are very sensitive to the negative charges on molecules in TCNQ-based CT compounds, the charge transfer degree (DCT) could be estimated from $c/(b+d)$ values: [15-16]

$\mathrm{DCT} = (\alpha_{\mathrm{CT}} - \alpha_0)/(\alpha_{-1} - \alpha_0)$

Where $\alpha_x = c/(b+d)$, the subscripts of CT, 0, and -1 indicate the CT complex, the neutral molecule, and the anion, respectively. The bond lengths, $c/(b+d)$ values and predicted DCT are summaried in Table S1.

Table S1. Bond Lengths, $c/(b+d)$ values and predicted DCT values of F_4TCNQ in different states.

	a (Å)	b (Å)	c (Å)	d (Å)	$c/(b+d)$	DCT
F_4TCNQ	1.333(2)	1.436(2)	1.371(8)	1.433(2)	0.4779	0
F_4TCNQ [17]	1.356(4)	1.414(4)	1.415(4)	1.430(6)	0.4975	1
TMF4TQ	1.339	1.437	1.382	1.441	0.4802	0.13

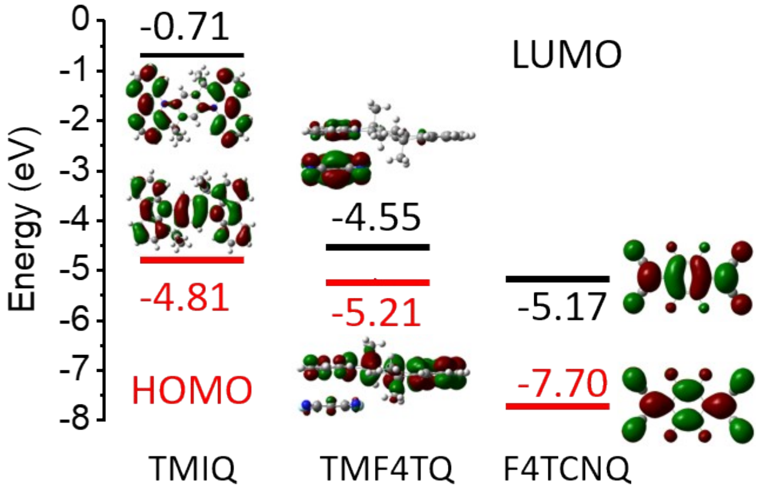

Figure S7. MO energy-level diaram of TMIQ, F_4TCNQ and the TMF4TQ and their corresponding electron density distributions calculated on Gaussian 09 program at the level of B3LYP/6-31G**.

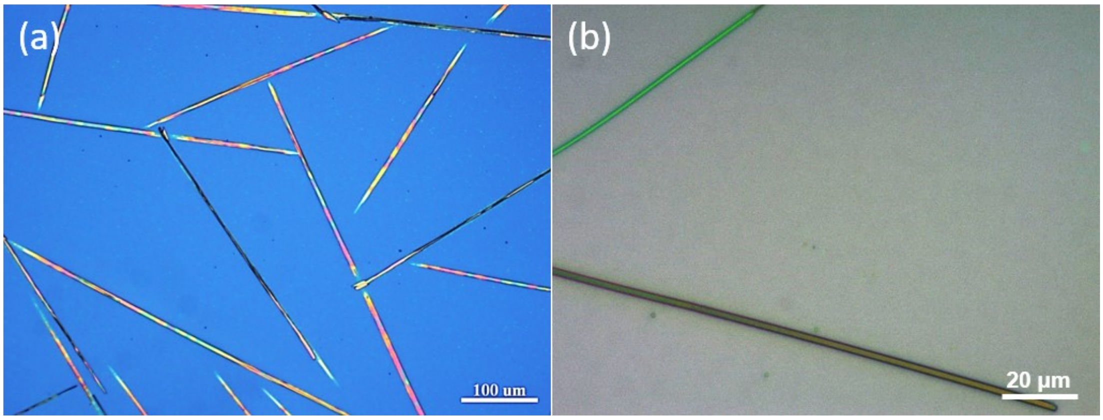

Figure S8. Optical micrographs of microcrystals for (a) TMIQ and (b) TMF4TQ self-assembled on the OTS-modified SiO_2/Si substrates from CH_2Cl_2 solution.

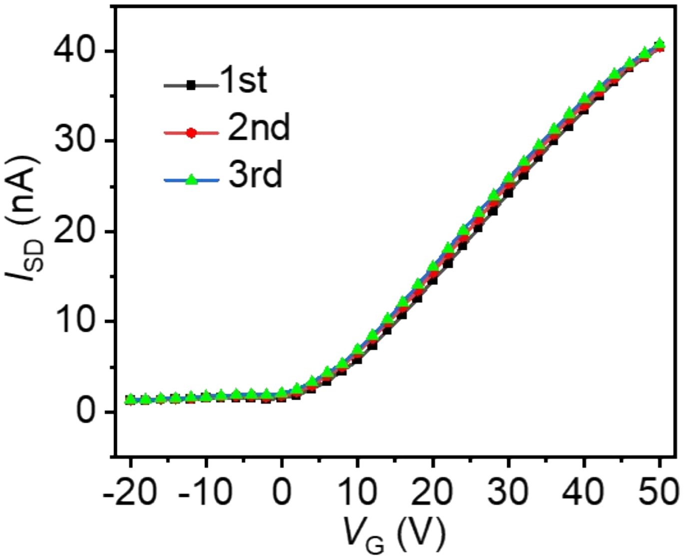

Figure S9. The repeated transfer characteristic measurements for device based on TMF4TQ microcrystal in air with relative humidity range 50% ~ 75%.

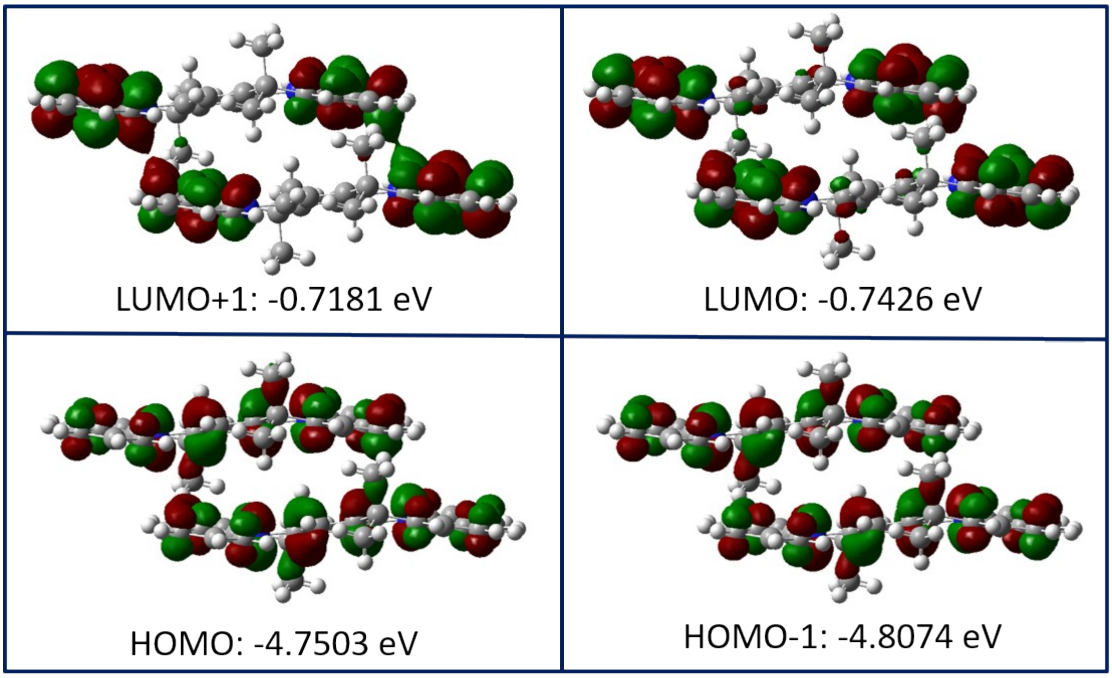

Figure S10. Energy-splitting method estimated transfer integrals along π-π stacking directions in crystal TMIQ. $t_{\mathrm{hole}} = (E_{\mathrm{H}}\text{-}E_{\mathrm{H-1}})/2 = 28.57$ meV, $t_{\mathrm{electron}} = (E_{\mathrm{L+1}}\text{-}E_{\mathrm{L}})/2 = 12.25$ meV.[14, 18-19]

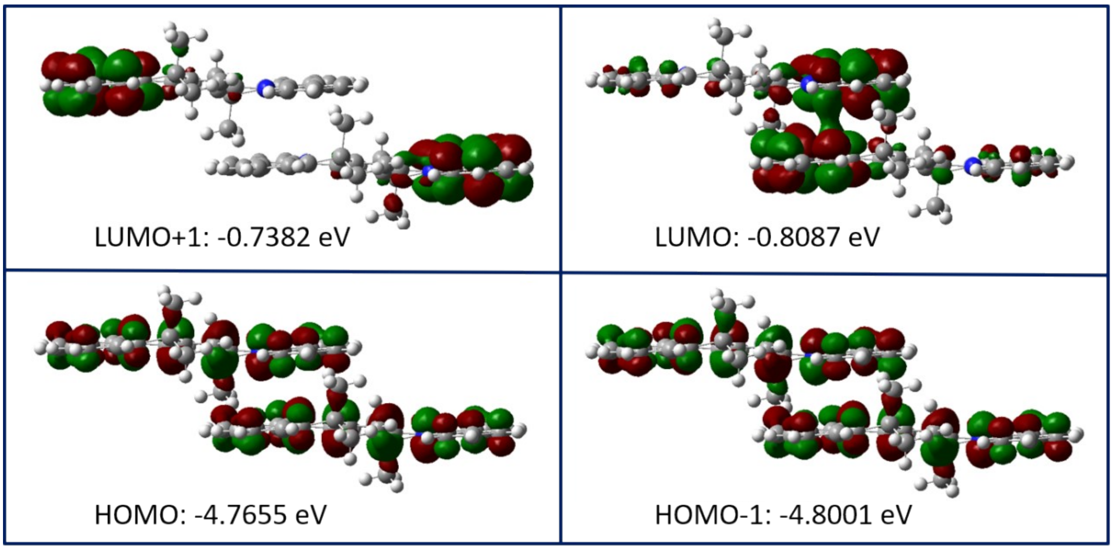

Figure S11. Energy-splitting method estimated transfer integrals in D-D directions along π-π stacking in cocrystal of TMF4TQ. $t_{\mathrm{hole}} = (E_{\mathrm{H}}-E_{\mathrm{H-1}})/2 = 17.28$ meV, $t_{\mathrm{electron}} = (E_{\mathrm{L+1}}-E_{\mathrm{L}})/2 = 35.24$ meV.[14, 18-19]

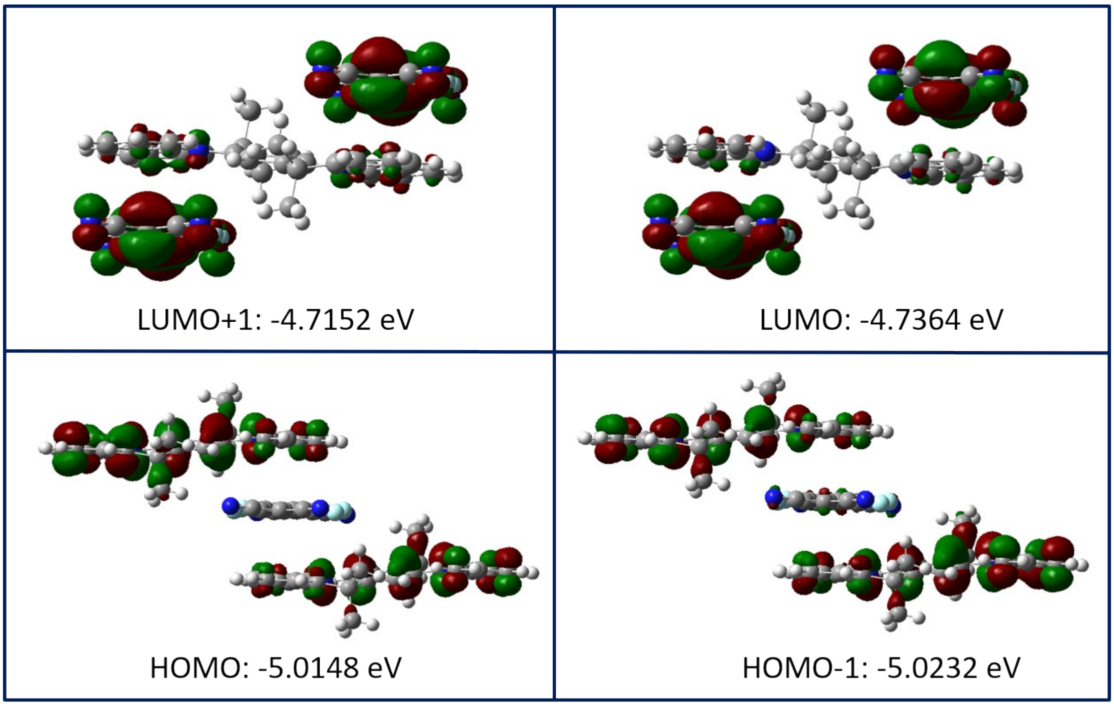

Figure S12. Energy-splitting method estimated transfer integrals along mixed stacking directions (D-A-D/A-D-A) in cocrystal of TMF4TQ. $t_{\mathrm{hole}} = (E_{\mathrm{H}}-E_{\mathrm{H-1}})/2 = 4.218$ meV, $t_{\mathrm{electron}} = (E_{\mathrm{L+1}}-E_{\mathrm{L}})/2 = 21.22$ meV. [14, 18-19]

Table S2. Crystallographic data and structure refinement parameters of TMIQ and TMF4TQ.

Name	TMIQ	TMF4TQ
Empirical formula	$C_{36}H_{28}N_2$	$C_{48}H_{28}F_4N_6$
Formula weight	488.60	764.76
Temperature (K)	295	100(2)
Wavelength (Å)	0.71073 (Mo K α)	0.71073 (Mo K α)
Crystal system	Monoclinic	Triclinic
Space group	P21/c	P-1
Cell Length (Å)	a 6.4601(11)	a 8.9947(4)
	b 22.900(3)	b 10.5212(4)
	c 8.6053(14)	c 10.7845(4)
Cell Angle (^{o})	α 90^{o}	α 79.6858(13)^{o}
	β 98.884(8)^{o}	β 67.3649(12)^{o}
	γ 90^{o}	γ 68.3715(14)^{o}
Cell Volume (Å^3)	1257.8(3)	874.84(6)
Z	2	1
μ (mm^{-1})	0.075	0.102
Dc (g/cm^3)	1.290	1.452
F (000)	516.0	394
Theta range for data collection	2.98 to 25°	2.69 to 33.74°
Index ranges	7<=h<=-9, 32<=k<=-32, 12<=l<=-11	-14<=h<=13, -16<=k<=16, -16<=l<=10
R_1 [$I > 2\sigma(I)$]	0.0849	0.0664
wR2 [$I > 2\sigma(I)$]	0.1344	0.1278
GOF	1.0635	1.051

[1] Bourhis, L.J., Dolomanov, O.V., Gildea, R.J., Howard, J.A.K., Puschmann, H. *Acta Cryst.* 2015, **A71**, 59-75.

[2] Dolomanov, O.V., Bourhis, L.J., Gildea, R.J, Howard, J.A.K. & Puschmann, H. *J. Appl. Cryst.* 2009, **42**, 339-341.

[3] Sheldrick, G.M. *Acta Cryst.* 2015, **A71**, 3-8.

[4] G. M. Sheldrick, SADABS—Bruker AXS Area Detector Scaling and Absorption, 2008.

[5] G. M. Sheldrick, *Acta Crystallogr., Sect. A:* 2015, **A71**, 3–8.

[6] G. M. Sheldrick, *Acta Crystallogr., Sect. C.* 2015, **C71**, 3–8.

[7] L. Jiang, J. Gao, E. Wang, H. Li, Z. Wang, W. Hu, L. Jiang, *Adv. Mater.* 2008, **20**, 2735-2740.

[8] A. D. Becke, *Phys. Rev. A*, 1988, **38**, 3098–3100.

[9] C. T. Lee, W. T. Yang and R. G. Parr, *Phys. Rev. B*, 1988, **37**, 785–789.

[10] A. D. Becke, *J. Chem. Phys.*, 1993, **98**, 5648–5652.

[11] M. J. Frisch, G. W. Trucks, H. B. Schlegel, G. E. Scuseria, M. A. Robb, J. R. Cheeseman, G. Scalmani, V. Barone, G. A. Petersson, H. Nakatsuji, X. Li, M. Caricato, A. Marenich, J. Bloino, B. G. Janesko, R. Gomperts, B. Mennucci, H. P. Hratchian, J. V. Ortiz, A. F. Izmaylov, J. L. Sonnenberg, D. Williams-Young, F. Ding, F. Lipparini, F. Egidi, J. Goings, B. Peng, A. Petrone, T. Henderson, D. Ranasinghe, V. G. Zakrzewski, J. Gao, N. Rega, G. Zheng, W. Liang, M. Hada, M. Ehara, K. Toyota, R. Fukuda, J. Hasegawa, M. Ishida, T. Nakajima, Y. Honda, O. Kitao, H. Nakai, T. Vreven, K. Throssell, J. A. Montgomery, J.

E. P. Jr., F. Ogliaro, M. Bearpark, J. J. Heyd, E. Brothers, K. N. Kudin, V. N. Staroverov, T. Keith, R. Kobayashi, J. Normand, K. Raghavachari, A. Rendell, J. C. Burant, S. S. Iyengar, J. Tomasi, M. Cossi, J. M. Millam, M. Klene, C. Adamo, R. Cammi, J. W. Ochterski, R. L. Martin, K. Morokuma, O. Farkas, J. B. Foresman, D. J. Fox, *Gaussian 09, Revision A.02*, Gaussian, Inc., Wallingford CT, **2016**.

[12] G. B. Bacskay, *Chem. Phys.*, 1981, **61**, 385–404.

[13] A. Schäfer, C. Huber and R. Ahlrichs, *J. Chem. Phys.*, 1994, **100**, 5829–5835.

[14] Z. Wang, F. Yu, J. Xie, J. Zhao, Y. Zou, Z. Wang, Q. Zhang, *Chem.-Eur. J.* 2020, **26**, 3578-3585.

[15] H. Jiang, P. Hu, J. Ye, K. K. Zhang, Y. Long, W. Hu, C. Kloc, *J. Mater. Chem. C* 2018, **6**, 1884-1902.

[16] P. Hu, K. Du, F. Wei, H. Jiang, C. Kloc, *Cryst. Growth Des.* 2016, **16**, 3019-3027.

[17] Z. G. Soos, H. J. Keller, K. Ludolf, J. Queckbörner, D. Wehe, S. Flandrois, *J. Chem. Phys.* 1981, **74**, 5287-5294.

[18] M. Ottonelli, M. Piccardo, D. Duce, S. Thea, G. Dellepiane, *Energy Procedia* 2012, **31**, 31-37.

[19] E. F. Valeev, V. Coropceanu, D. A. da Silva Filho, S. Salman, J. L. Brédas, *J. Am. Chem. Soc.* 2006, **128**, 9882-9886.